JOURNAL OF THEORETICAL AND APPLIED MECHANICS
61, 1, pp. 49-63, Warsaw 2023
https://doi.org/10.15632/jtam-pl/157571

IMPACT OF MATERIAL NONLINEARITY OF DAM-FOUNDATION ROCK SYSTEM ON SEISMIC PERFORMANCE OF CONCRETE GRAVITY DAMS

Djamel Ouzandja

Laboratory of Materials and Mechanics of Structures (LMMS), Department of Civil Engineering, University of Msila, Algeria

e-mail: djamel.ouzandja@univ-msila.dz

Mokhtar Messaad

Laboratory of Hydraulic Developments and Environment LAHE, University of Biskra, Algeria

e-mail: mokhtar.messaad@univ-biskra.dz

Amina T. Berrabah

Department of Civil Engineering and Public Works, Faculty of Technology, University Belhadj Bouchaib, Ain Temouchent, Algeria

e-mail: a.taharberrabah@gmail.com

Mohamed Belhrizi

Consultant, Antony, France

e-mail: mohambel@free.fr

This paper shows the impact of material nonlinearity of a dam-foundation rock system on seismic performance of Oued Fodda concrete gravity dam, located at northwestern side of Algeria. For the purpose, a three-dimensional dam-foundation rock system finite element model is employed in analyses. The hydrodynamic interaction between reservoir water and dam-foundation system is implicitly taken into consideration by the Westergaard approach using surface finite elements added to dam-fluid and foundation-fluid interfaces. The concrete material model is used to present the cracking of dam concrete under a seismic load the using smeared crack approach based on the Willam and Warnke failure criterion. The materially nonlinear analysis for both dam concrete and foundation rock is performed using Drucker--Prager model. According to numerical results, tensile stresses and maximum strains reduce significantly in the materially nonlinear model. In addition, the cracking areas in the dam decrease also when material nonlinearity characteristics of the dam-foundation rock system is considered in analyses.

Keywords: concrete gravity dam, dynamic dam-foundation rock interaction, Drucker-Prager model, cracking, nonlinear earthquake analysis, finite element method

1. Introduction

The dynamic response analysis of concrete gravity (CG) dams is influenced by a number of factors; among them there is soil-structure interaction, fluid-structure interaction and material nonlinear performance of a dam-foundation rock system itself. Burman *et al.* (2008) studied the response of CG dams to seismic loading considering foundation rock nonlinearity. The results illustrated that nonlinear behavior of foundation rock affected the dam response. The influence of materially nonlinear properties of Sariyar gravity dam exposed to near-fault seismic movements was performed by Akköse and Şimeşk (2010). The study demonstrated that the concrete dam nonlinearity gave a significant impact on the dam-water-foundation system response. Burman *et al.* (2010) presented seismic analysis of a dam-foundation system considering the effect

of materially nonlinear foundation domain. The taking into account of the nonlinear material response of foundation rock generates higher displacements and stresses in the dam compared to the results extracted from linear analysis. Wang *et al.* (2015) used linear and nonlinear computation approaches to study seismic behavior of CG dams considering the effect of integrated duration. Ouzandja and Tiliouine (2015) investigated the effect of conditions of contact at the dam-foundation interface on seismic behavior of Oued Fodda CG dam employing linear and nonlinear analyses. Their results showed that nonlinear analysis led to lower responses. Yazdani and Alembagheri (2017) utilized material and geometric nonlinearities to study the seismic response of Pine Flat dam. Khazaei-Poul and Zerva (2018) conducted nonlinear seismic analyses of CG dams considering the influence of foundation rock.

In three-dimensional (3D) models, Wang *et al.* (2012) investigated seismic nonlinear performance of CG dams including dam-foundation interaction. An earthquake nonlinear analysis of roller-compacted concrete (RRC) dams was presented by Kartal (2012) considering the friction contact formulation at the dam-foundation-reservoir interface. The results indicated that displacements increase in the materially nonlinear response, whereas the principal stress components decrease, in contrast, under hydrodynamic pressure. Hariri-Ardebili (2014) revealed the effect of foundation rock nonlinearity on the stability of concrete dams subjected to earthquakes. His study showed that considering the nonlinear model of foundation rock increases the response and damaged area in the dam. Arici *et al.* (2014) and Yilmazturk *et al.* (2015) presented nonlinear seismic studies on a RCC dam using 2D and 3D models. The results illustrated that 3D analysis of the dam was significantly different from that resulted from 2D analysis. This comparative study revealed the necessity and importance of taking into account 3D analysis as these gravity structures are constructed in relatively narrow canyons for seismic safety assessment. A materially nonlinear analysis of CG dams considering the dynamic fluid-structure interaction was performed by Ouzandja *et al.* (2017). Wang *et al.* (2017) studied seismic damage of Guandi gravity dam using hard and soft contact models. The study was based on transient nonlinear seismic analyses. A linear and nonlinear earthquake performance of Cine RCC dam was investigated by Kartal and Karabulut (2018). Larger tensile stresses were noticed in linear analysis according to their study. Moradloo *et al.* (2018) studied seismic damage of arch concrete dams through transient nonlinear analysis. Their results manifested that the index of displacement failure was more conservative and impractical in the assessment of seismic damage than the index of tensional failure. Karabulut and Kartal (2020) exposed the impact of boundary conditions on earthquake response of a RCC dam in linear and nonlinear analyses. They found that the dam performance increases under effects of viscous boundary conditions. The influence of earthquake epicenter distance on the fracture response of concrete dams was examined by Karalar and Çavuşli (2020). The study demonstrated that the dam nonlinear seismic response depends on the epicenter distance of the earthquake. Pirooznia and Moradloo (2021) presented seismic cracking of concrete arch dams using a nonlinear dynamic model considering dam-reservoir interaction.

The current paper exhibits the impact of material nonlinearity of a dam-foundation rock interaction system on the response of CG dams during earthquake. To this end, a 3D finite element model of the dam-foundation rock system is employed in different analyses using the ANSYS software (2018). Oued Fodda CG dam, located in Chlef town at northwestern Algeria, is chosen in this study. The added mass approach (Westergaard, 1933) is used to model the hydrodynamic effect of the reservoir fluid using 3D surface finite elements that are applied on the dam-fluid and foundation-fluid interfaces. The concrete material model, available with element Solid65, is used to predict seismic cracking of dam concrete due to a multiaxial stress state using the smeared crack approach based on the Willam and Warnke (1975) failure criterion. The Drucker-Prager criterion (Drucker and Prager, 1952) is selected in a materially nonlinear response for the dam-foundation rock coupled system.

2. Drucker-Prager model

The Drucker-Prager model (Drucker and Prager, 1952) is widely used in finite element numerical modeling codes, especially dedicated to geotechnical and geomechanical applications. This model represents a simple approach of materials behavior with internal friction, coherent or not (soils, rocks, concrete and various granular materials). The Drucker-Prager criterion is a generalization of the von Mises criterion for materials with internal friction. The failure surface representing the von Mises criterion is a cylinder parallel to the trisector of the principal stress space. And that representing Drucker-Prager criterion is a cone with a circular section admitting the same axis as the symmetry axis (Fig. 1) (Chen and Mizuno (1990). The equation of this surface can be expressed as

$$f = \alpha I_1 + \sqrt{J_2} - k \tag{2.1}$$

where α and k are constants that depend on the angle of internal friction φ and cohesion c of the material presented by

$$\alpha = \frac{2\sin\varphi}{\sqrt{3}(3-\sin\varphi)} \qquad k = \frac{6c\cos\varphi}{\sqrt{3}(3-\sin\varphi)} \tag{2.2}$$

in Eq. (2.1), I_1 is the first stress tensor invariant of σ_{ij} written as follows

$$I_1 = \sigma_{11} + \sigma_{22} + \sigma_{33} \tag{2.3}$$

and J_2 is the second invariant of the deviatoric stress tensor s_{ij} formulated by

$$J_2 = \frac{1}{2} s_{ij} s_{ij} \tag{2.4}$$

where s_{ij} is the deviatoric stresses given as follows

$$s_{ij} = \sigma_{ij} - \delta_{ij}\sigma_m \qquad i,j = 1,2,3 \tag{2.5}$$

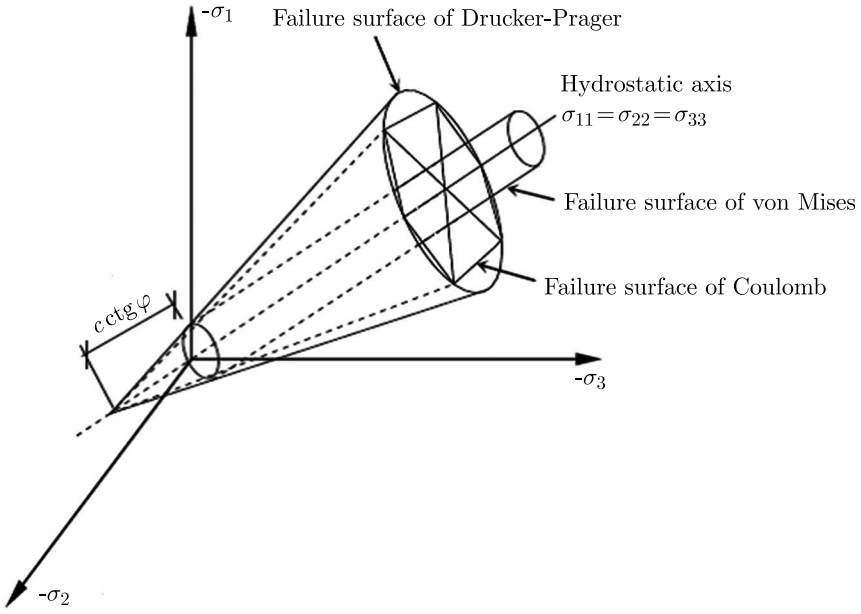

Fig. 1. Failure surface of Coulomb, Drucker-Prager and von Mises (Chen and Mizuno, 1990)

In Eq. (2.5), δ_{ij} is the Kronecker delta, which is equal to 1 for $i = j$; 0 for $i \neq j$, and σ_m is the mean stress given as

$$\sigma_m = \frac{I_1}{3} = \frac{\sigma_{11} + \sigma_{22} + \sigma_{33}}{3} = \frac{\sigma_{ii}}{3} \tag{2.6}$$

If the terms in Eq. (2.5) are determined by Eq. (2.6) and replaced in Eq. (2.4), the second invariant of the deviatoric stress tensor can be presented as follows

$$J_2 = \frac{1}{6}[(\sigma_{11} - \sigma_{22})^2 + (\sigma_{22} - \sigma_{33})^2 + (\sigma_{33} - \sigma_{11})^2] + \sigma_{12}^2 + \sigma_{13}^2 + \sigma_{23}^2 \tag{2.7}$$

3. Numerical model

3.1. Material properties

The numerical application treats Oued Fodda CG dam existing in Chlef territory at the northwest of Algeria, which is classified as high seismic activity zone in the national seismic code. This region suffered a strong earthquake known as the 1980 El Asnam earthquake (M7) that destroyed more than 70% of the city. The studied dam-foundation system is shown in Fig. 2.

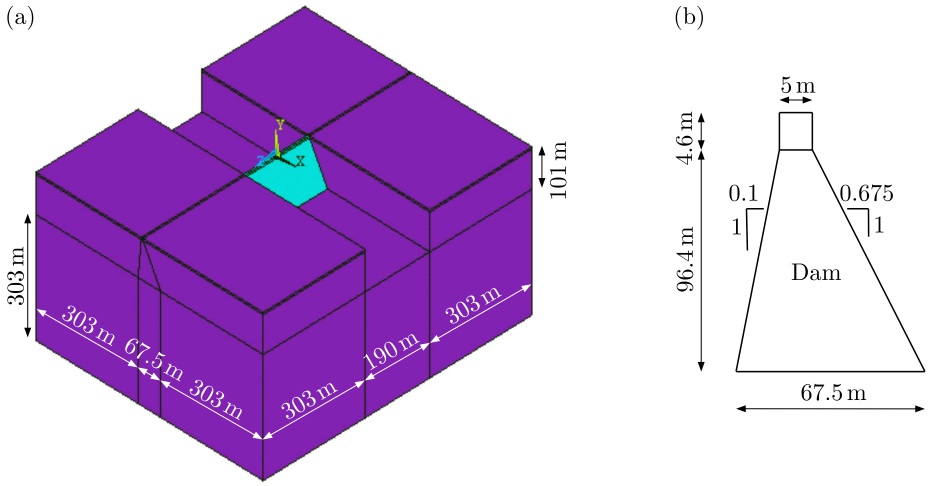

Fig. 2. Geometry of Oued Fodda dam-foundation rock system: (a) dam-foundation rock system, (b) dam

Mechanical properties of dam-foundation system materials are summarized in Table 1. Nonlinear analyses for both dam concrete and foundation rock are defined using the Drucker-Prager model (Drucker and Prager, 1952) (Table 1). The tensile and compressive strengths of dam concrete are 2.2 MPa and 24.1 MPa, respectively.

Table 1. Mechanical properties of the concrete dam and its foundation rock

Material properties	Material	
	Concrete dam	Foundation rock
Modulus of elasticity [MPa]	24600	20000
Poisson's ratio	0.20	0.33
Mass density [kg/m^3]	2640	2000
Cohesion [MPa]	2.7	1.9
Angle of internal friction	37	28

3.2. Dam-foundation rock system discretization

The dam-foundation rock system is discretized with a 3D finite element model illustrated in Fig. 3 using ANSYS computer Code (2018). The model exhibits 39750 finite elements, among them 2700 solid elements (Solid65) employed for the dam, and 37050 solid elements (Solid45) considered for the foundation rock. The hydrodynamic effect of the reservoir fluid is modeled employing the Westergaard (1933) approach. This method, which is an approximate approach, replaces the fluid with mass distributed uniformly on the dam-fluid and foundation-fluid interfaces, i.e., the fluid is represented as structural masses added to that of the dam and foundation. In this study, 3D surface finite elements (Surf154) are used to model the added mass approach, resulting in 900 elements.

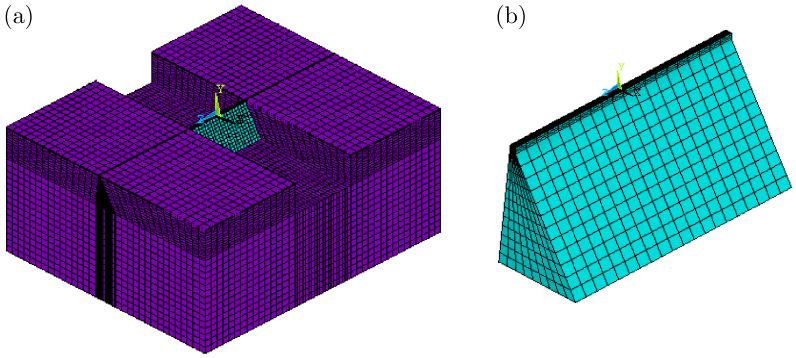

Fig. 3. Finite element discretization of Oued Fodda dam-foundation rock system: (a) dam-foundation rock system, (b) dam

4. Nonlinear seismic analyses of Oued Fodda dam-foundation rock system

This work shows the earthquake nonlinear response of Oued Fodda dam-foundation rock system. The dam region incurred a severe earthquake, 1980 El Asnam earthquake (M7), which caused significant material and human losses. However, there was available only seismic replica record of this earthquake. The stream direction was subjected to the horizontal component of the seismic replica record with peak ground acceleration (PGA) of 0.132 g, which was scaled by factor 2.5 to attain to a PGA of 0.33 g (Fig. 4) equal roughly to the evaluated PGA of the 1980 El Asnam earthquake (M7).

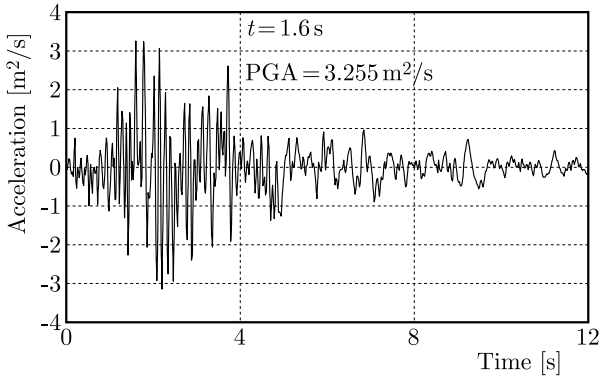

Fig. 4. Horizontal component of the 1980 El Asnam earthquake replica record after scaling operation of 2.5

Two different models are provided in earthquake analysis: the first model prescribes that the dam concrete is modeled using element Solid65 based on the smeared crack approach, whereas

the foundation rock is presumed to be elastic linear. The second model presents that the dam concrete is modeled using element Solid65 based on the smeared crack approach, while both the dam and foundation rock are modeled by an elastic-plastic model. The horizontal displacements, principal stress and strain components as well as cracking response resulted from the first and second models and are compared to each other.

4.1. Displacements

Figure 5 exhibits the distribution of horizontal displacements in upstream and downstream faces along the dam crest in the first and second models. The envelopes of maximum horizontal displacements of the dam during earthquake are presented in Fig. 6 for both two models. As can be shown from Figs. 5 and 6 that the horizontal displacements obtained from the second model are lower than those ones from the first model. Therefore, the material nonlinearity of the dam-foundation rock coupled system can lead to a decrease in the displacement response of the dam.

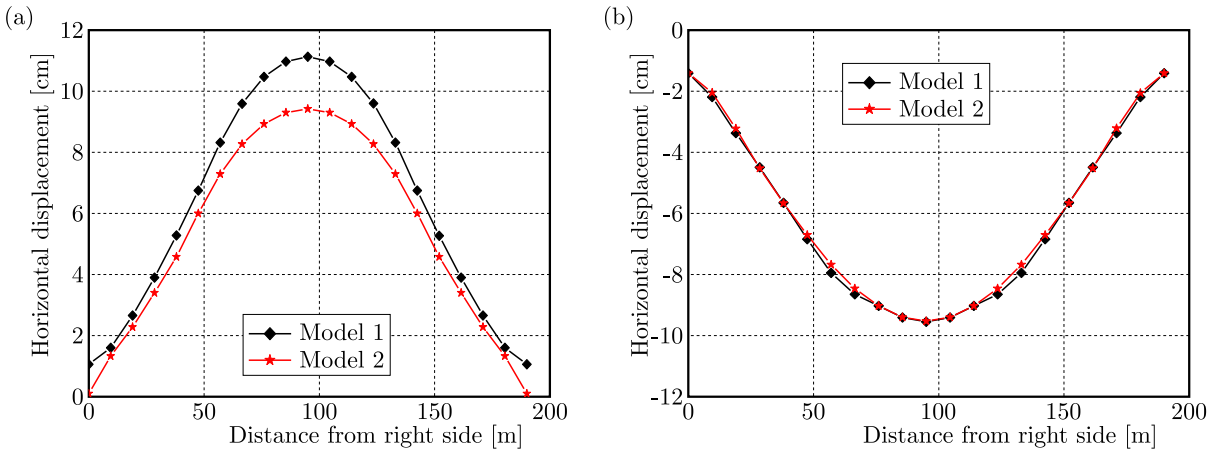

Fig. 5. Distribution of horizontal displacements in two faces along the dam crest: (a) downstream face, (b) upstream face

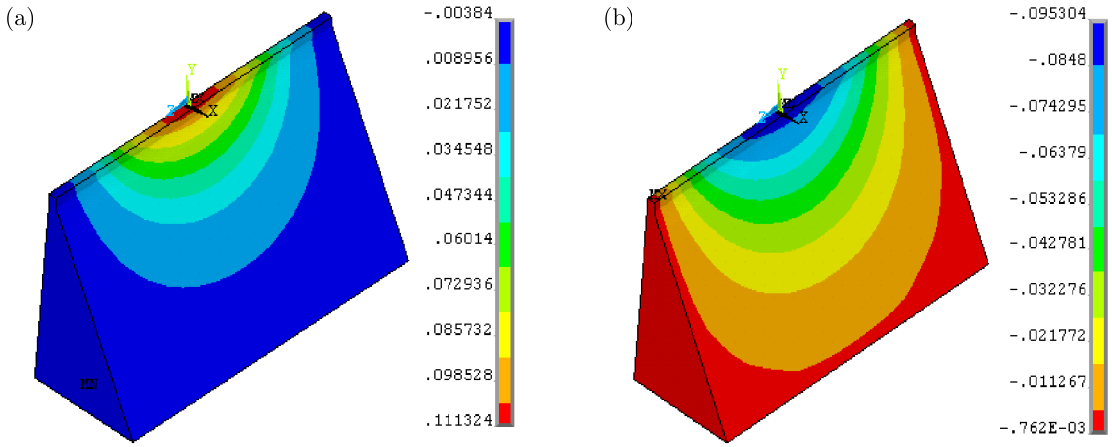

Fig. 6. Envelopes of maximum horizontal displacements for the dam, [m]: (a) model 1, (b) model 2

Figure 7 compares the horizontal displacement time history at the upstream middle crest located along the dam central axis, in which the maximum displacement at the crest decreases from 11.13 cm in the first model to 9.53 cm in the second one. This indicates a 14% reduction for the crest displacement amount in the second model. The horizontal displacement time history at

the heel and toe located along the dam symmetry central axis is plotted in Fig. 8. It is evident that the displacement time histories for both heel and toe of the dam in the first and second models are similar to each other, which the maximum displacement of 1.68 cm at the heel and 1.58 cm at the toe.

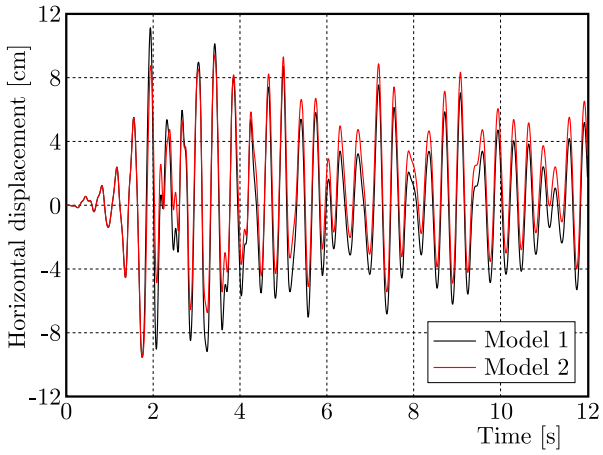

Fig. 7. Horizontal displcement time history at the dam crest for two models 1 and 2

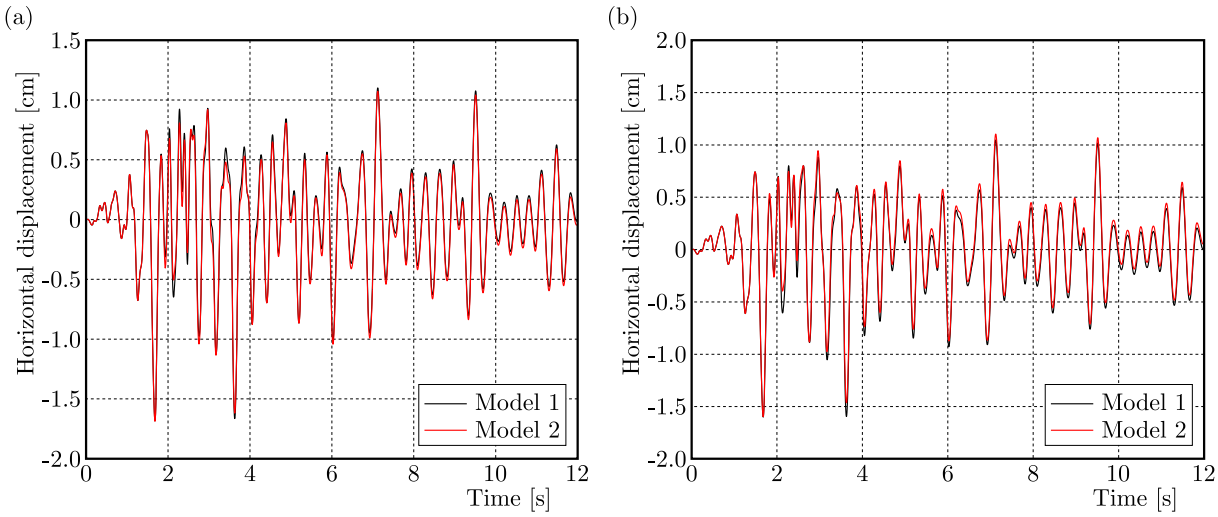

Fig. 8. Horizontal displacement time history at the heel and toe of the dam: (a) at the dam heel, (b) at the dam toe

4.2. Principal stresses

The envelopes of maximum principal tensile and compressive stresses in the upstream face of the dam appear in Figs. 9 and 10, respectively, for the two models. On the other hand, Figs. 11 and 12 show also the envelopes of principal stress components in the downstream face. As can be seen, the tensile stresses resulted from the second model are much lower than those from the first model, while the values of compressive stresses are convergent to each other. It is observed that the maximum principal stress components occur at right and left upper lateral extremities and middle bottom parts for both upstream and downstream faces in the two models.

The time history of principal stresses at the dam middle heel is presented in Fig. 13, in which the maximum principal tensile stress reduces from 11254.74 kN/m^2 in the first model to 3747.09 kN/m^2 in the second one. This denotes a decrease of 67% for the amount of principal tensile stress in the second model. In contrast, the value of maximum compressive stress is

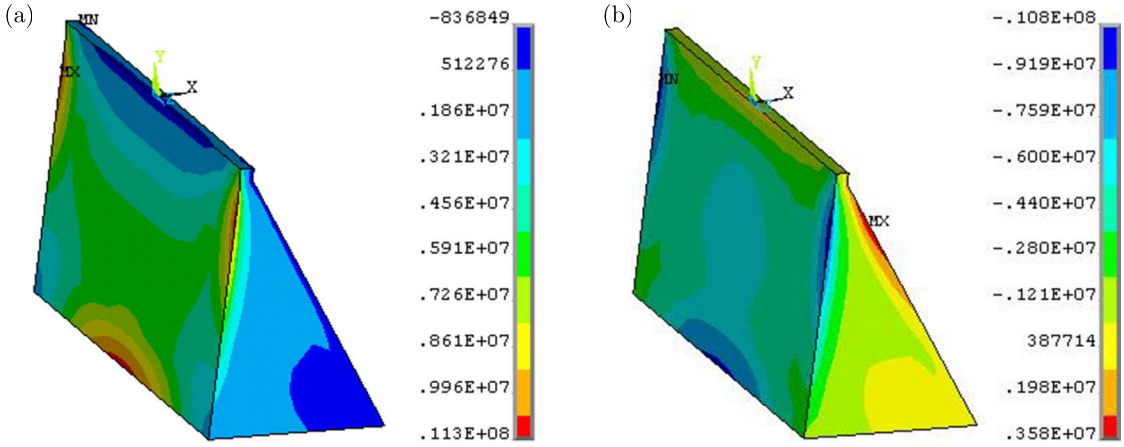

Fig. 9. Envelopes of maximum principal tensile stresses in the dam upstream face, [Pa]: (a) model 1, (b) model 2

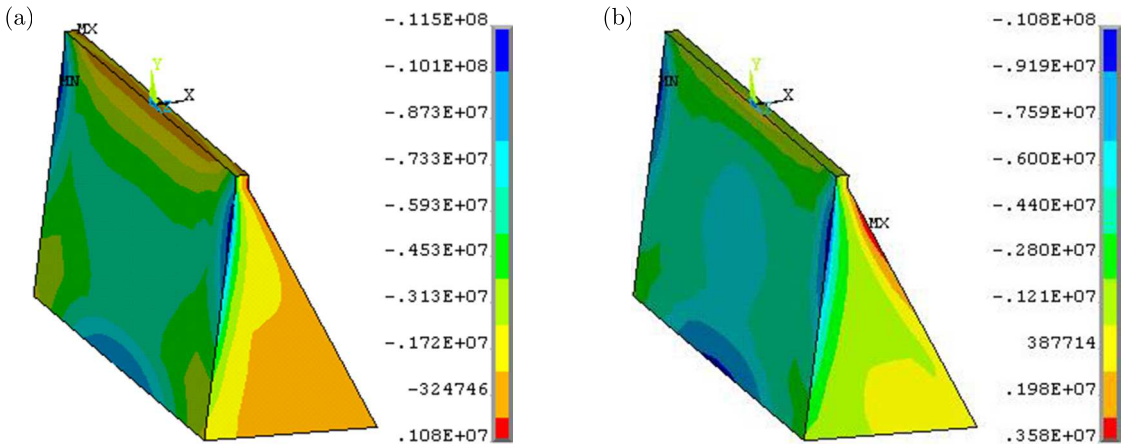

Fig. 10. Envelopes of maximum principal compressive stresses in the dam upstream face, [Pa]: (a) model 1, (b) model 2

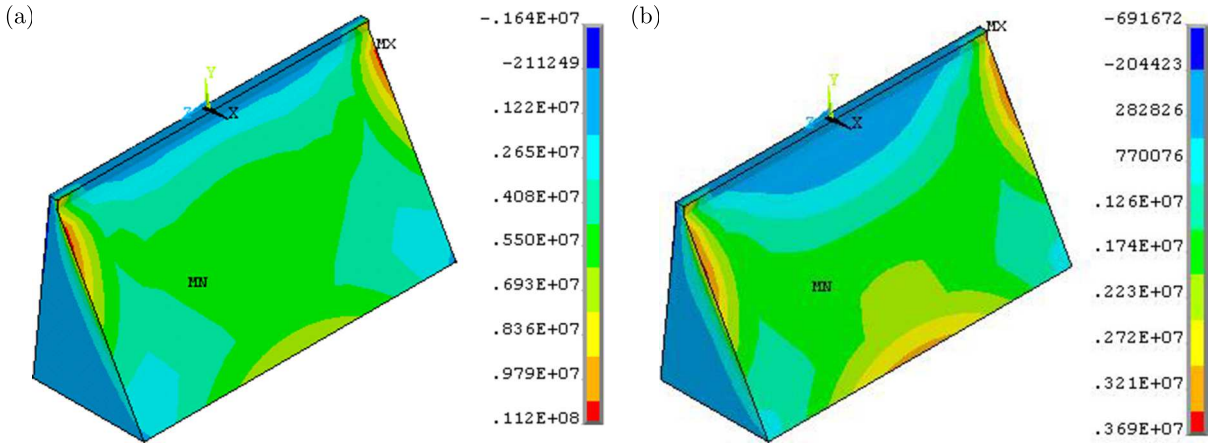

Fig. 11. Envelopes of maximum principal tensile stresses in the dam downstream face, [Pa]: (a) model 1, (b) model 2

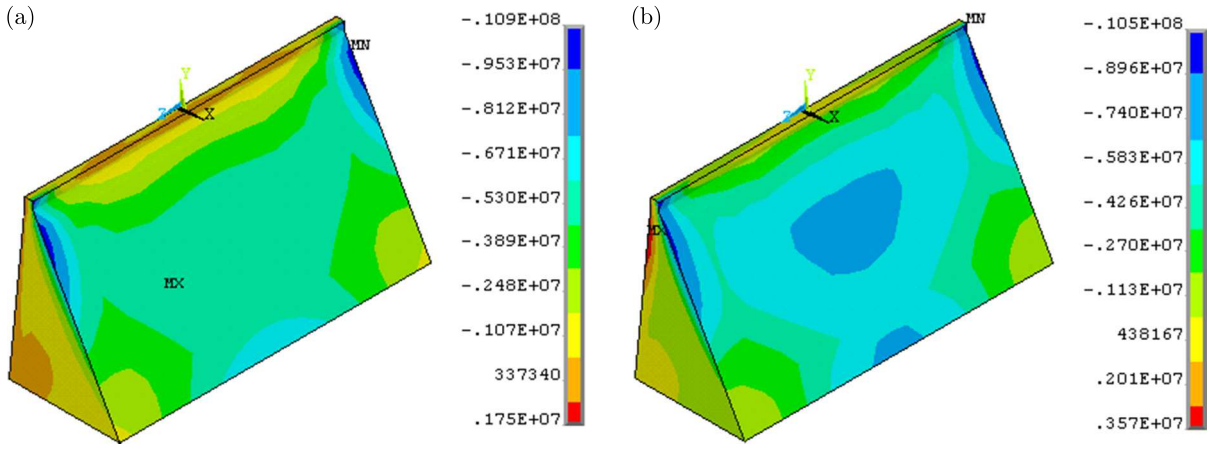

Fig. 12. Envelopes of maximum principal compressive stresses in the dam downstream face, [Pa]: (a) model 1, (b) model 2

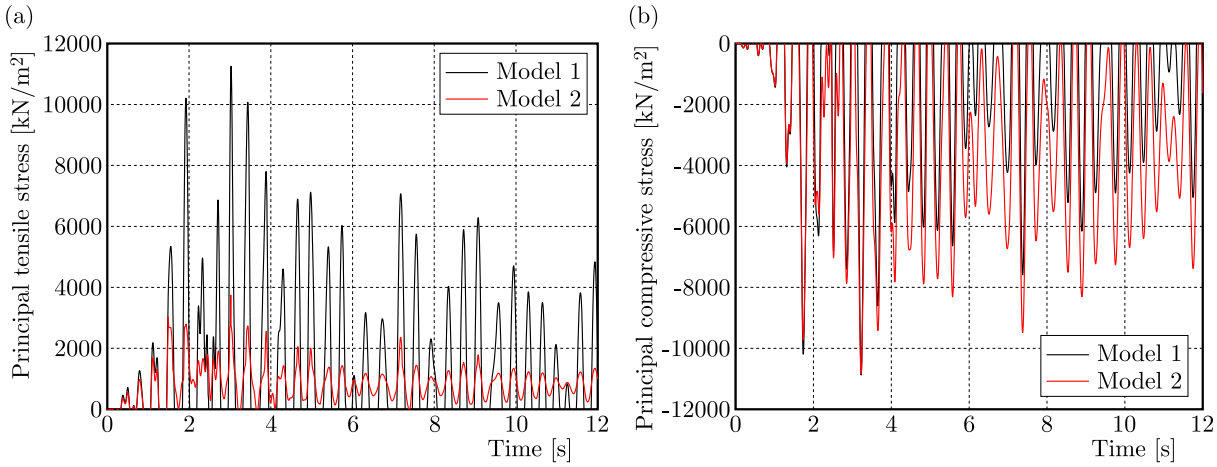

Fig. 13. Time history of principal stresses at the dam heel: (a) principal tensile stress, (b) principal compressive stress

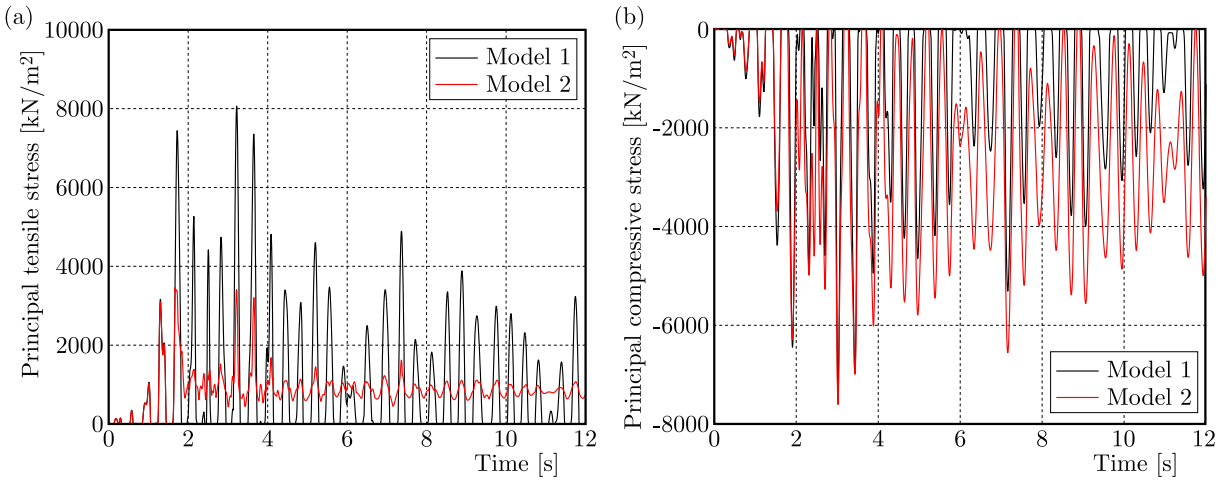

Fig. 14. Time history of principal stresses at the dam toe: (a) principal tensile stress, (b) principal compressive stress

convergent in the two models and equal to $-10874.37\,\mathrm{kN/m^2}$. According to Fig. 14 illustring the time history of maximum principal stresses at the middle toe, the maximum principal tensile stress decreases from $8065.77\,\mathrm{kN/m^2}$ in the first model to $3457.57\,\mathrm{kN/m^2}$ in the second analysis, i.e, a diminution of 43% for the amount of principal tensile stress in the second model. In contrast, the value of maximum compressive stress is convergent in the two models and equal to $-7604.92\,\mathrm{kN/m^2}$.

4.3. Principal strain

The envelopes of maximum and minimum principal strains in the dam upstream face are depicted in Figs. 15 and 16, respectively, for both two models. On the other hand, Figs. 17 and 18 illustrate also the envelopes of principal strain components in the downstream face. As can be shown, the maximum principal strains found from the second model are much lower than those from first one, whereas the values of minimum strains are convergent to each other. It is obvious that the maximum principal strain components appear where the maximum principal stress components occur.

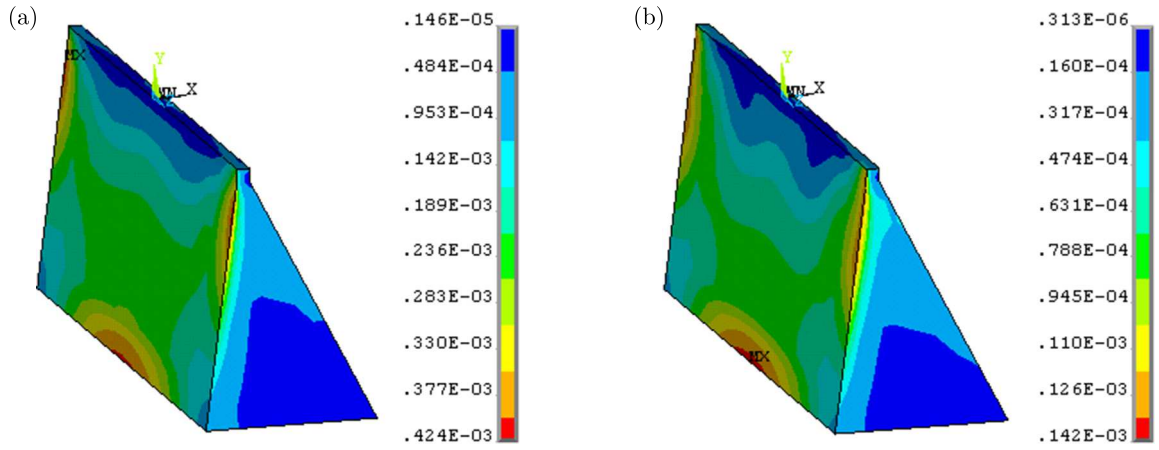

Fig. 15. Envelopes of maximum principal strain in the dam upstream face, [m/m] : (a) model 1, (b) model 2

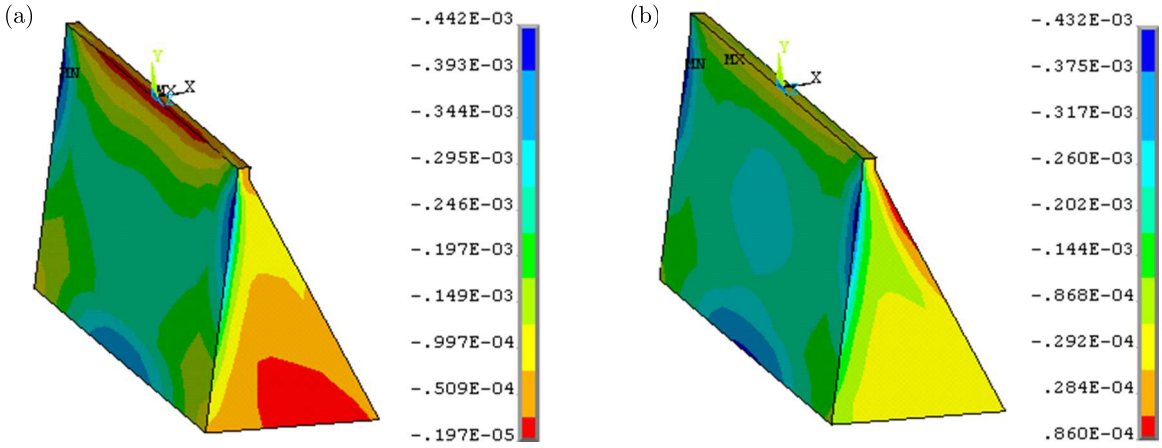

Fig. 16. Envelopes of minimum principal strain in the dam upstream face, [m/m]: (a) model 1, (b) model 2

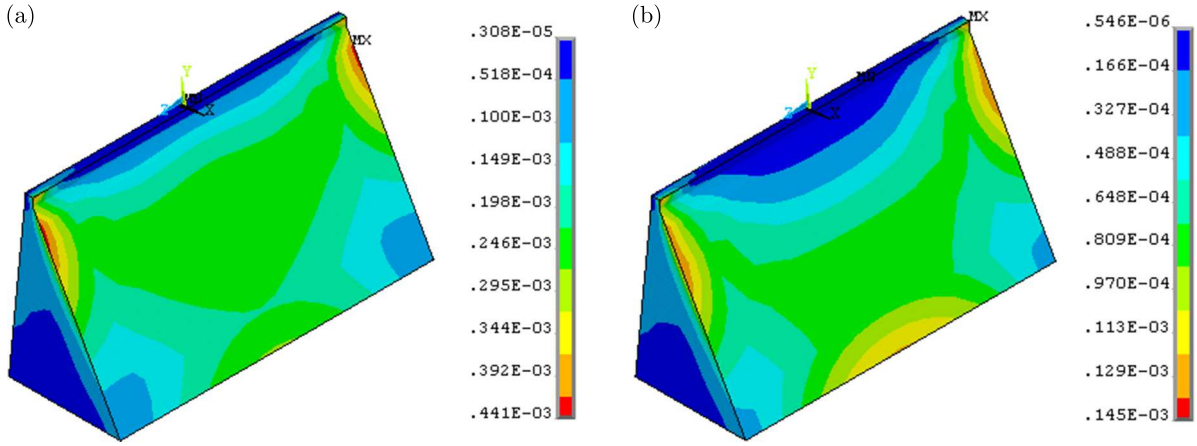

Fig. 17. Envelopes of maximum principal strain in the dam downstream face, [m/m]: (a) model 1, (b) model 2

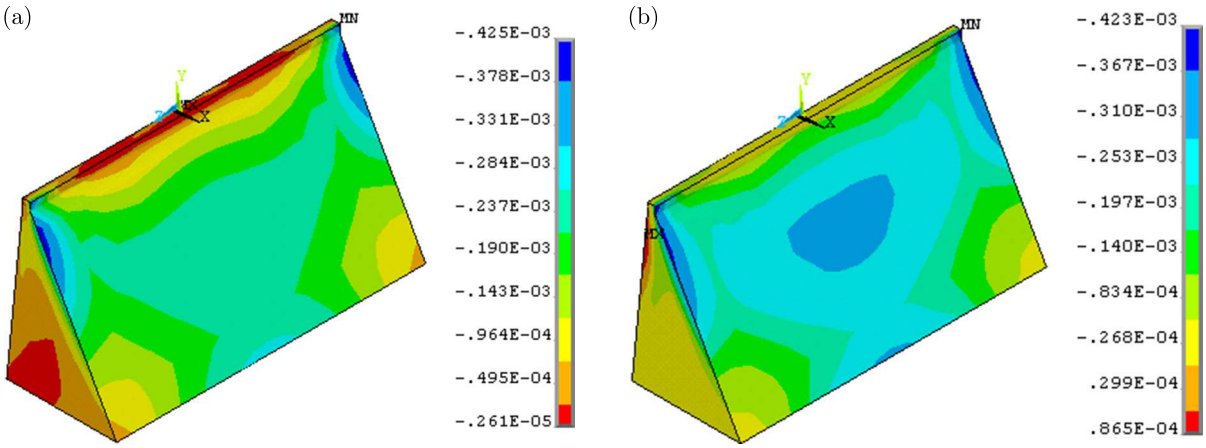

Fig. 18. Envelopes of minimum principal strain in the dam downstream face, [m/m]: (a) model 1, (b) model 2

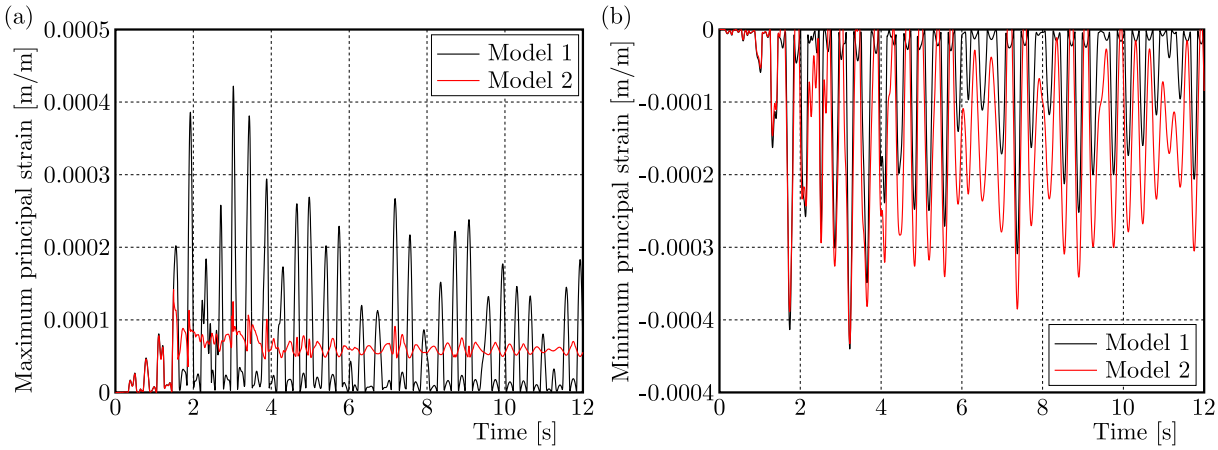

Fig. 19. Time history of principal strains at the dam heel: (a) maximum principal strain, (b) minimum principal strain

The time history of principal strains at the dam heel is compared in Fig. 19, in which the maximum principal strain decreases from 0.422‰ in the first model to 0.141‰ in the second one. In contrast, the value of minimum strain is convergent in the two models and is equal to −0.437‰. According to Fig. 20 representing the time history of principal strains at the toe, the maximum principal strain reduces from 0.313‰ in the first model to 0.130‰ in the second one. In contrast, the value of minimum strain is convergent in the two models and is equal to −0.318‰.

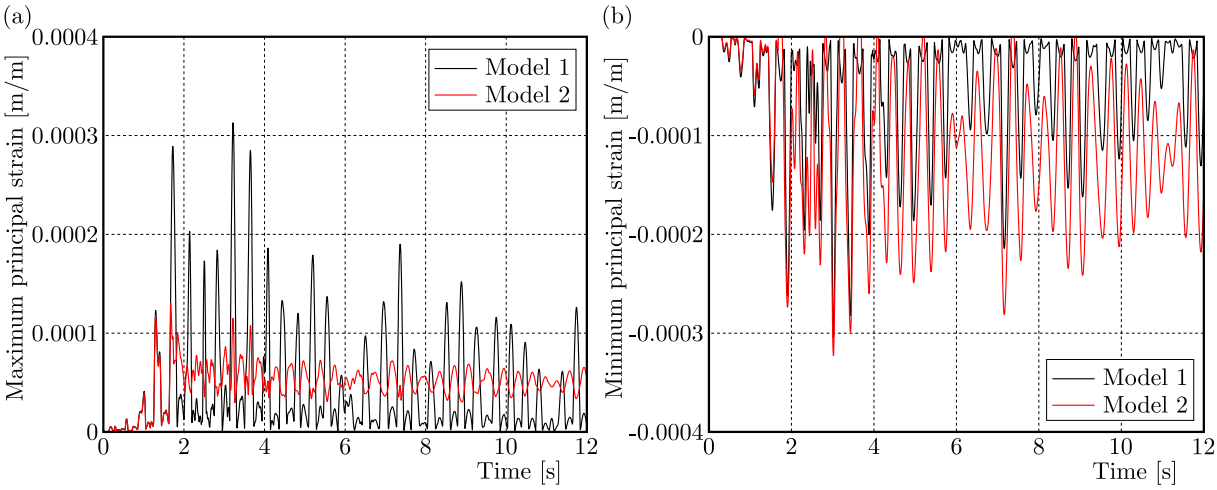

Fig. 20. Time history of principal strains at the dam toe: (a) maximum principal strain, (b) minimum principal strain

4.4. Cracking profiles

The final cracking profiles in upstream and downstream faces of Oued Fodda dam are shown in Figs. 21 and 22, respectively, for both models. As may be seen, cracks occur in tensioned parts in two models, where the maximum tensile stresses appear. In the second model, the cracks occur at the right and left upper lateral extremities and middle bottom parts for both upstream and downstream faces, while the cracking includes large parts on upstream and downstream faces in the first model according to the distribution of maximum principal tensile stresses into the dam faces (see Figs. 9a and 11a). These big cracked areas affect significantly stability and safety of the dam structure. In general, the materially nonlinear properties of the dam and foundation rock can significantly reduce damage areas in the dam body.

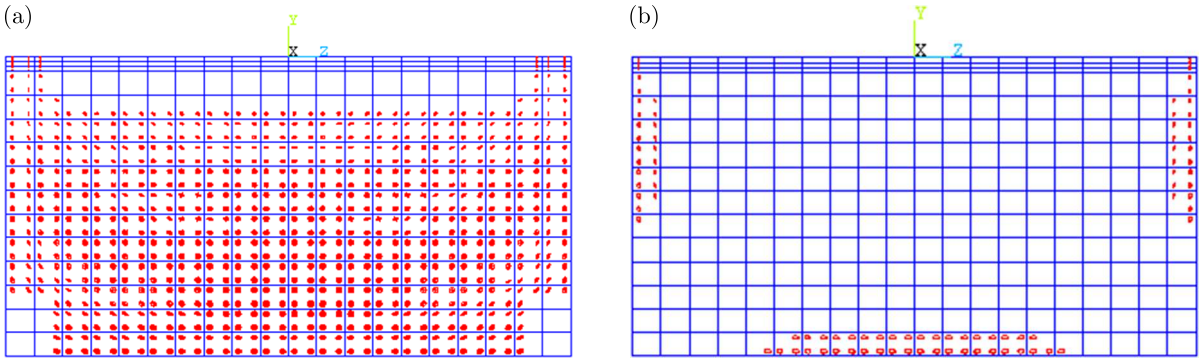

Fig. 21. Cracking profile in the dam upstream face: (a) model 1, (b) model 2

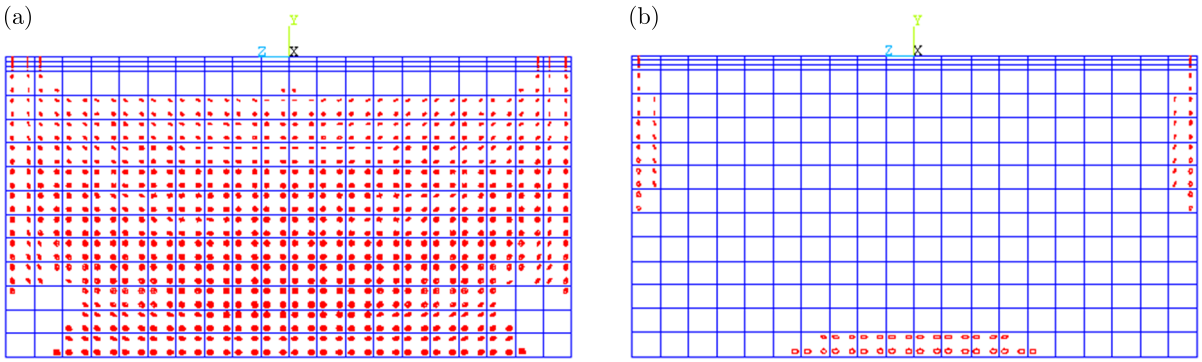

Fig. 22. Cracking profile in the dam downstream face: (a) model 1, (b) model 2

5. Conclusions

The current study presents the effect of material nonlinearity of both the dam and foundation rock on the earthquake response of Oued Fodda dam. The hydrodynamic interaction between the reservoir water and dam-foundation system is modeled by the Westergaard approach using 3D surface finite elements. The Drucker-Prager criterion is employed in materially nonlinear analysis for the dam-foundation rock coupled system. From this numerical investigation, one can obtain the following inferences:

1. The tacking into account the materially nonlinear model of the dam-foundation rock coupled system can:
   - lead to a decrease in the horizontal displacements of the dam,
   - significant decrease in the tensile stresses and maximum strains in the dam,
   - reduction of cracked areas in the dam body.
2. The dam real behavior is obtained in the second model, which is a more realistic model, compared to the first one.
3. The results obtained from this study demonstrate the need for a substantially nonlinear model of the coupled dam-foundation rock system in order to assess the design and to predict the dam reliable earthquake performance.
4. The material nonlinearity should be taken into account in numerical analyses to achieve more reliable and practical findings.

According to this study, taking into account the materially nonlinear model of the dam--foundation coupled system can have an impact on displacements, magnitude of tensile stresses and failure zones in concrete of the dam. In order to achieve reliable, accurate and realistic findings of the seismic performance of the dam-foundation coupled system, it has therefore become crucial and necessary to do substantially nonlinear analysis.

References

1. Akköse M., Şimşek E., 2010, Non-linear seismic response of concrete gravity dams to near--fault ground motions including dam-water-sediment-foundation interaction, *Applied Mathematical Modelling*, **34**, 11, 3685-3700

2. ANSYS, 2018, Theory User's Manual, Swanson Analysis Systems Inc., Canonsburg, PA, USA

3. Arici Y., Binici B., Aldemir A., 2014, Comparison of the expected damage patterns from two- and three-dimensional nonlinear dynamic analyses of a roller compacted concrete dam, *Structure and Infrastructure Engineering*, **10**, 3, 305-315

4. Burman A., Maity D., Sreedeep S., 2010, Iterative analysis of concrete gravity dam-nonlinear foundation interaction, *International Journal of Engineering, Science and Technology*, **2**, 4, 85-99

5. Burman A., Reddy B.V., Maity D., 2008, Seismic analysis of concrete gravity dams considering foundation flexibility and nonlinearity, *Proceedings of the 12th International Conference on Computational Methods and Advances in Geomechanics (IACMAG)*, Goa, India.

6. Chen W.F., Mizuno E., 1990, *Nonlinear Analysis in Soil Mechanics*, Elsevier, Amsterdam

7. Drucker D.C., Prager W., 1952, Soil mechanics and plastic analysis or limit design, *Quarterly of Applied Mathematics*, **10**, 2, 157-165

8. Hariri-Ardebili M.A., 2014, Impact of foundation nonlinearity on the crack propagation of high concrete dams, *Soil Mechanics and Foundation Engineering*, **51**, 2, 72-82

9. Karabulut M., Kartal M.E., 2020 Seismic analysis of Roller Compacted Concrete (RCC) dams considering effect of viscous boundary conditions, *Computers and Concrete*, **25**, 3, 255-266

10. Karalar M., Çavuşli M., 2020, Seismic effects of epicenter distance of earthquake on 3D damage performance of CG dams, *Earthquakes and Structures*, **18**, 2, 201-213

11. Kartal M.E., 2012, Three-dimensional earthquake analysis of roller-compacted concrete dams, *Natural Hazards and Earth System Sciences*, **12**, 7, 2369-2388

12. Kartal M.E., Karabulut M., 2018, Earthquake performance evaluation of three-dimensional roller compacted concrete dams, *Earthquakes and Structures*, **14**, 2, 167-178

13. Moradloo J., Naserasadi K., Zamani H., 2018, Seismic fragility evaluation of arch concrete dams through nonlinear incremental analysis using smeared crack model, *Structural Engineering and Mechanics*, **68**, 6, 747-760

14. Ouzandja D., Tiliouine B., 2015, Effects of dam-foundation contact conditions on seismic performance of concrete gravity dams, *Arabian Journal for Science and Engineering*, **40**, 11, 3047-3056

15. Pirooznia A., Moradloo A.J., 2021, Seismic fracture analysis of concrete arch dams incorporating the loading rate dependent size effect of concrete, *Structural Engineering and Mechanics*, **79**, 2, 169-198

16. Khazaei-Poul M., Zerva A., 2018, Nonlinear dynamic response of concrete gravity dams considering the deconvolution process, *Soil Dynamics and Earthquake Engineering*, **109**, 324-338

17. Wang G., Wang Y., Lu W., Yu M., Wang C., 2017, Deterministic 3D seismic damage analysis of Guandi concrete gravity dam: A case study, *Engineering Structures*, **148**, 263-276

18. Wang G., Wang Y., Lu W., Zhou W., Zhou C., 2015, Integrated duration effects on seismic performance of concrete gravity dams using linear and nonlinear evaluation methods, *Soil Dynamics and Earthquake Engineering*, **79**, 223-236

19. Wang H., Feng M., Yang H., 2012, Seismic nonlinear analyses of a concrete gravity dam with 3D full dam model, *Bulletin of Earthquake Engineering*, **10**, 6, 1959-1977

20. Westergaard H.M., 1933, Water pressures on dams during earthquakes, *Transactions of the American Society of Civil Engineers (ASCE)*, **98**, 2, 418-433

21. Willam K.J., Warnke E.D., 1975, Constitutive model for the triaxial behavior of concrete, *Proceedings of International Association for Bridge and Structural Engineering*, **19**, 174, ISMES, Bergamo, Italy

22. Yazdani Y., Alembagheri M., 2017, Nonlinear seismic response of a gravity dam under near-fault ground motions and equivalent pulses, *Soil Dynamics and Earthquake Engineering*, **92**, 621-632

23. Yilmazturk S.M., Arici Y., Binici B., 2015, Seismic assessment of a monolithic RCC gravity dam including three dimensional dam-foundation-reservoir interaction, *Engineering Structures*, **100**, 137-148

Manuscript received August 7, 2022; accepted for print October 26, 2022